# Parameter Extraction for a Microwave Micromachined Switch

Jinghong Chen, Karen M. Coperich, Sung-Mo (Steve) Kang, and Jose Schutt-Aine

Department of Electrical and Computer Engineering
University of Illinois at Urbana-Champaign
1308 W. Main St., Urbana, IL 61801

## ABSTRACT

This paper details new parameter extraction methods for microwave micromachined switches. Specifically new methods for extracting switch turn-on and turn-off transient behavior and switch electromagnetic behavior are discussed. The accuracy of these methods are verified by comparison between simulation results and experimental measurements.

***Keywords***: micromechanical switch, transient simulation, S-parameter, modeling.

## INTRODUCTION

Micromechanical switches have demonstrated great potential at microwave frequencies due to their very low distortion, low power, and low "on-state" insertion loss characteristics. Such switches are often characterized by metrics of switching speed and also electromagnetic properties. To study switching speed and its sensitivity to switch geometry scaling and material properties, a nonlinear, dynamic, lumped model has been developed. The model takes into account the effect of mass inertia, electrostatic actuation, viscoelasticity damping, residual stress and the external actuating circuit. To predict the behavior of the micromachined switch at microwave frequencies, a method of moments based, static, 3-D capacitance extraction algorithm was formulated. The switch electromagnetic behavior is captured in terms of the extracted capacitances. The S-parameter simulation is also performed based on the equivalent capacitance circuit of the switch. These extracted models not only provide good design guidance for switch structure design but also can be efficiently used in a system-level simulator for transient and steady-state simulation. Modeling and simulation results will be shown to correlate very well with measurement data.

## TRANSIENT SIMULATION

One of the critical electromechanical properties of micromechanical switches is the switching speed. Mechanical switches are inherently slower than electronic switches, with switching speed in the microsecond to millisecond range. Switching speed has become the main limitation of such switches and it is important to study how materials and construction can affect the switching speed. In the past, both lumped models and 3-D finite element models [1-2] have been developed to study switch transient characteristics. 3-D finite element simulation is useful to examine more detailed geometry effects, but are mostly limited to static analysis and are computationally expensive making them difficult to use for system level simulation. In this paper, we focus on lumped modeling and will use the TI switch structure [3], as shown in Fig.1, to illustrate the modeling concept. The methodology can also be applied to other switch structures.

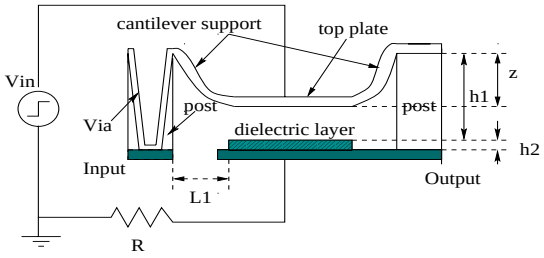


Figure 1: Schematic sketch of a MEMS switch.

Unlike the approach used in [3], where the switch is lumped modeled as a single rigid parallel-plate capacitor suspended above a fixed ground plate by an ideal linear spring, we observed that it is more accurate to model the support cantilever and the top membrane of the switch separately. This permits the model to be scalable. In our analysis, we have modeled the top membrane of the switch as a rigid diaphragm supported above the ground plate by two cantilevers. For small deflections, the spring constant of the cantilever, $k$, is given by, $k = (12EI/L_1^3)$, where $w$, $t$, and $L_1$ represent cantilever width, thickness, and length. $I = (wt^3/12)$ is the cantilever moment of the inertia. $E$ is the material Young's modulus. The relationship between the applied voltage and the support cantilever beam deflection can be obtained by equating the electrostatic force due to the applied voltage to the restoring support cantilever spring forces as follows,

$$2kz = \varepsilon_0 A \frac{V^2}{2(h_1 + \frac{h_2}{\kappa} - z)^2} \quad (1)$$

where $\varepsilon_0$ is the permitivity of free space, $\kappa$ is the di-

electric constant of the thin dielectric layer above the bottom plate, $A$ is the overlap area between the top and bottom plates. The dimensions $h_1$, $h_2$, and $z$ are shown in Fig.1. This gives us a relationship for the applied voltage as,

$$V(z) = (h_1 + \frac{h_2}{\kappa} - z)\sqrt{\frac{48EI}{\varepsilon_0 A L_1^3} z} \quad (2)$$

Equation (2) has been plotted in Fig.2 as a function of $z/h_1$, the gap closure percentage. From the curve, we observed that for top plate closure from zero to about one-third of the initial gap, the applied voltage required to hold the beam increases in a monotonic way and the system is stable in this region. For gap closure greater than one-third of the initial spacing, the system becomes unstable since less voltage is required to hold the top plate at a greater cantilever deflection. The top plate will snap down to close the switch at this voltage.

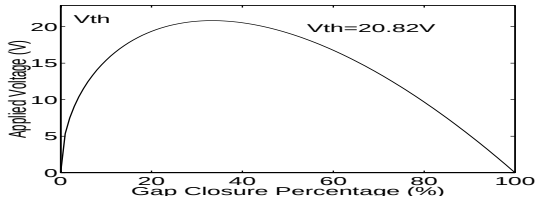


Figure 2: Relationship between applied voltage and top plate displacement. Parameters are: $L_1$=30$\mu m$, $w$=30$\mu m$, $t$=0.3$\mu m$, top plate diameter $D$=300$\mu m$, $h_1$=4$\mu m$, $E$=138$Gpa$, and $V_{in}$=30$V$.

The threshold voltage can be simply approximated by substituting $z=(h_1 + \frac{h_2}{\kappa})/3$ into (2) and from which an analytical formula of the threshold voltage can be obtained. The sensitivities of the threshold voltage with switch material properties and geometry constructions can thus be studied. One important observation of this study is that the pull-in threshold voltage is inversely proportional to the top plate membrane radius.

To model switch dynamic characteristics, and also including the squeezed-film damping effect, the equation of motion for the switch system is given by,

$$\frac{1}{2}\frac{\varepsilon_0 A}{(h_1 + \frac{h_2}{\kappa_0} - z)^2}V^2 - \frac{2 * 12EI}{L_1^3}z - \eta\frac{dz}{dt} = m\frac{d^2z}{d^2t} \quad (3)$$

where $\eta$ is the viscoelasticity constant, and $m$ is the mass of the top plate membrane. Considering the electric actuating circuit, we also have,

$$R\left[\frac{\varepsilon_0 A}{(h_1 + \frac{h_2}{\kappa} - z)}\frac{dV}{dt} + V\frac{\varepsilon_0 A}{(h_1 + \frac{h_2}{\kappa} - z)^2}\frac{dz}{dt}\right] + V = V_{in} \quad (4)$$

Equation (3) and (4) completely characterize the mechanical motion and electrical actuation of the switch system. By solving these coupled equations with proper initial conditions, the switch turn-on and turn-off dynamic behavior can be obtained. Simulation results using the same switch parameters as listed in Fig.2 are shown in Fig.3, which agrees well with the data published by [3]. The sensitivity of switching speed to switch geometrical and material peoperties such as cantilever beam length, initial gapping, top plate membrane radius, top plate thickness, material Young's modulus, and viscoelasticity damping are also investigated. Some of the simulation results are shown in Fig.4 to Fig.6. From this, we observed: 1) reducing the initial gapping, using materials with smaller Young's Modulus, and reducing the viscoelasticity damping can greatly speed up the switch turn-on times; 2) smaller top plate membrane thickness results in faster turn-on, but larger membrane thickness results in faster turn-off, optimal membrane thickness can be derived for composite turn-on and turn-off consideration; 3) turn-on times are almost invariant with variations of cantilever beam length, but the turn-off times are reduced with smaller cantilever beam length; 4) larger top-plate overlap area results in faster turn-on, but smaller top-plate overlap area can greatly speed up the turn-off time. The design tradeoffs within process limitations are evident.

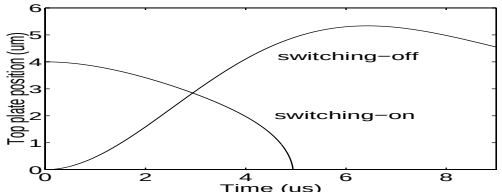


Figure 3: Switch turn-on and turn-off behavior.

We have used the guided-end beam model [4] to model the cantilever support instead of using the cantilever beam model as in [5]. This affects the values of the cantilever residual stress and thus the calculation of the switching time. The guided-end beam model seems to be a better match to our measurements. The switch pull-in effect as shown in Fig.3 is also more evident. In our simulation, a threshold value, specified by a $S_{21}$ parameter, as discussed in the next section can also be used to give a better definition of switch turning-off instead of arbitrarily defining switch turning-off as that the switch returns to its original position. We also applied the same modeling methodology to simulate a switch structure similar to the one developed at Rockwell [6]. Such a switch is also fabricated by the MicroLab at the University of Illinois. Fig.7 shows its structure. Simulation results agree well with experimental measurements of these devices. We conclude that for structures which are nearly parallel and which undergo only small deflections prior to pull-in, as is the case for MEMS switches, our lumped model is accurate and very useful in the design process. It explicitly provides a coupled system of equa-

tions which describes the switching speed and threshold voltage in terms of material properties and dimensions.

## MICROWAVE SIMULATION

In order to predict the behavior of the switch at microwave frequencies, the electromagnetic behavior of MEMS switches is captured in terms of circuit parameters. A method of moments based (MoM), static, 3-D capacitance extraction algorithm was specifically formulated to efficiently handle multiple planar layered regions which are common for MMIC device layouts. Embedded within the MoM formulation is the Green's function that describes the field response, at all locations/layers, due to an infinitesimal source. The Green's function can be written in either the spatial or spectral domain. The salient feature of our 3-D capacitance extractor is its real exponential approximation of the spectral domain Green's function,

$$K_j(\gamma) \simeq \sum_{i=1}^{M} f_i(\gamma) = \sum_{i=1}^{M} C_i e^{\gamma \lambda_i} \tag{5}$$

This approximation eliminates the nested infinite summations inherent to the analytic expression of the Green's function thereby turning it into a closed-form expression. Additionally, most of the spectral domain terms can be calculated based solely on the dielectric layer properties, independent of the metallic geometry. It was discovered that the accuracy of the exponential terms, $C_i$ and $\lambda_i$ , required double precision. The precision of these coefficients turned out, in most instances, to be more important than the actual number of terms used in the approximating sum.

To begin modeling a three-dimensional, $N$-conductor, metallic structure, surfaces must first be discretized with a mesh generator; then, test voltages are individually applied at each subsurface to compute induced charges. Capacitance values, $N^2$ total, can be computed after summing the total charge accumulation due to $N$ linearly independent voltage excitations. The elements of this matrix, $C_{ij}$ , dictate the relationship between $Q_i$, the total charge on conductor $i$, resulting from a voltage, $V_j$, applied to conductor $j$ when $V_{k \neq j} = 0$ as expressed in the equations below,

$$\begin{bmatrix} Q_1 \\ Q_2 \\ Q_3 \end{bmatrix} = \begin{bmatrix} C_{11} & C_{12} & C_{13} \\ C_{21} & C_{22} & C_{23} \\ C_{31} & C_{32} & C_{33} \end{bmatrix} \begin{bmatrix} V_1 \\ V_2 \\ V_3 \end{bmatrix} \tag{6}$$

As a result, the off-diagonal elements of the capacitance matrix are negative. The conductors held at zero potential must have an induced charge whose sum total is equal and opposite to the positive charge accumulated on the excited conductor. The results also exhibit the diagonal symmetry required by reciprocity. Due to the spatial symmetry of the switch the capacitance matrix is further simplified as illustrated below,

$$\begin{bmatrix} C_{11} & C_{12} & C_{13} \\ C_{21} & C_{22} & C_{23} \\ C_{31} & C_{32} & C_{33} \end{bmatrix} \Rightarrow \begin{bmatrix} A & E & G \\ E & B & F \\ G & F & D \end{bmatrix} \Rightarrow \begin{bmatrix} A & E & G \\ E & B & E \\ G & E & B \end{bmatrix} \tag{7}$$

where, the later part is due to the physical symmetry of the switch geometry. It is vital that the schematic representation used in the frequency-domain simulation be consistent with the definitions used in the extraction. As a result, the values $C_{ij}$ are not directly transferable to the circuit diagram. The $N$x$N$ capacitance matrix must be converted into an equivalent $N$-node circuit. Self and mutual capacitances as defined in (8) must first be calculated.

$$C_{S_{ii}} = C_{ii} - \sum_{i=1}^{N} C_{M_{ij}} \qquad C_{M_{ij}} = -C_{ij} \tag{8}$$

In order to understand how the circuit represents $Q_i = C_{ij}V_j$, observe that if nodes 2 and 3 are grounded, the device reduces to $C_{S_{11}}$ in parallel with $C_{M_{12}}$ and $C_{M_{13}}$ which is equivalent to $C_{11}$ from the electromagnetic extraction program.

The switch depicted in Fig.7 was constructed by suspending a $20\mu m$ wide metallic strip $3\mu m$ above a GaAs substrate. The metallic contacts etched on the substrate are open-ended CPW as shown in Fig.7. The equivalent circuit in Fig.9 does not include inductances or resistive elements. This omission is not out of neglect. Inductive effects become significant for lengths of line on the order of a wavelength. The intended frequency of operation for the switch of Fig.7 is 77 GHz, which corresponds to a wavelength of $3.9mm$. Since the length of the longest metallic feature (i.e. the top bar of the switch) is no longer than $160\mu m$ for any of the three configurations studied, inductors will not be included in the RF model. The metallic depositions are gold in order to avoid losses and thereby resistive modeling parameters. The accuracy of the simulations will justify these assumptions.

The extracted capacitance matrices are shown in Fig.8 for the three slightly different switch configurations indicated below.

| switch type | overlap area | gap length |
|---|---|---|
| A | $200(\mu m^2)$ | $150(\mu m)$ |
| B | $600(\mu m^2)$ | $100(\mu m)$ |
| C | $200(\mu m^2)$ | $100(\mu m)$ |

Hewlett Packard's MDS microwave circuit simulator was used to simulate the equivalent circuit model of the switch. A graph of the resulting S-parameter simulation is plotted along with the corresponding measurements in Fig.10. The capacitance extraction and S-parameter simulations of the equivalent circuit appear to satisfactorily predict the measured $S_{11}$ and $S_{21}$ parameters. In the off state, the two ports of the switch are highly isolated as indicated by $S_{21} < -30dB$ in both the measurement and simulation data. The non-smoothness of the

measured $S_{21}$ date is most likely due to the fact that the signal level is approaching the noise floor. Using a general two-port S-parameter model, the MEMS switch can then be inserted into a circuit simulator to perform frequency domain steady-state simulations together with MMIC components.

## CONCLUSION

In conclusion, new methods have been developed for extracting the electromechanical and microwave properties for micromachined switches. Simulation results correlate well with measurement data. These extracted models can be embedded into a circuit simulator for transient and steady-state simulation to optimize switch material and structure for circuit applications.

## REFERENCES


[1] B.E. Artz, " A finite element method for determining structural displacements from electrostatic forces," 1992 IEEE Solid State Sensors and Actuators Workshop, pp. 190-193.

[2] K.E. Peterson, "Micromechanical membrane switches on silicon," IBM J. Res. Develop., vol. 23, pp. 376-385, 1979.

[3] C. Goldsmith, J.Randall, and T.H.Lin, "Characteristics of Micromachined Switches at Microwave Frequencies," 1996 IEEE MTT-S Digest, pp.1141-1144.

[4] G.K. Fedder, "Simulation of Micromechanical Systems," PhD dissertation, UC-Berkeley, 1994.

[5] E.K. Chan, R.W. Dutton, and P.M. Pinsky, "Nonlinear Dynamic Modeling of Micromachined Microwave Switch," 1997 MTT-S. 1511-1514.

[6] S.C. Shen, "RF MEMS switches," Techanical Report, Microelectronic Lab, UIUC, 1998.

[7] K.S. Oh, and J.E. Schutt-Aine, "Capacitance Computations in Multilayered Dielectric Using the Closed-form Spatial Green Functions," IEEE Trans. MTT, vol.42, pp.1143-1453.


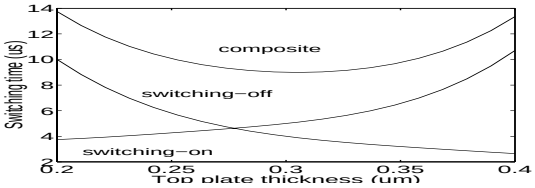


Figure 4: Switch turn-on and turn-off response vs. top plate thickness.

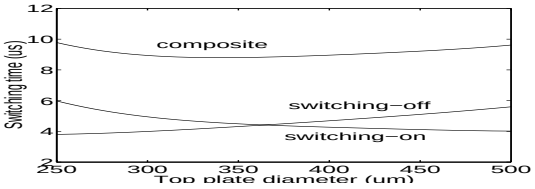


Figure 5: Switch turn-on and turn-off response vs. top plate radius.

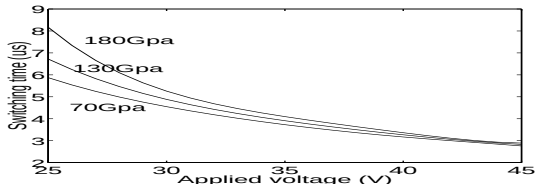


Figure 6: Switch turn-on and turn-off vs. different material Young Modulus.


Figure 7: A resistive MEMS switch structure.

$$\mathbf{C}_{\mathcal{A}} = \begin{bmatrix} 9.733E-15 & -9.50E-16 & -9.50E-16 \\ -9.50E-16 & 4.372E-14 & -7.62E-17 \\ -9.50E-16 & -7.62E-17 & 4.372E-14 \end{bmatrix} \text{Farads}$$

$$\mathbf{C}_{\mathcal{B}} = \begin{bmatrix} 8.576E-15 & -1.64E-15 & -1.64E-15 \\ -1.64E-15 & 4.4335E-14 & -1.322E-16 \\ -1.64E-15 & -1.322E-16 & 4.4335E-14 \end{bmatrix} \text{Farads}$$

$$\mathbf{C}_{\mathcal{C}} = \begin{bmatrix} 6.99E-15 & -9.68E-16 & -9.68E-16 \\ -9.68E-16 & 4.376E-14 & -1.34E-16 \\ -9.68E-16 & -1.34E-16 & 4.376E-14 \end{bmatrix} \text{Farads}$$

Figure 8: Extracted capacitance for three slightly different switch configurations.

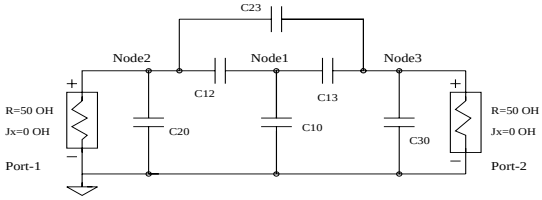


Figure 9: Equivalent capacitance circuit of the MEMS switch.

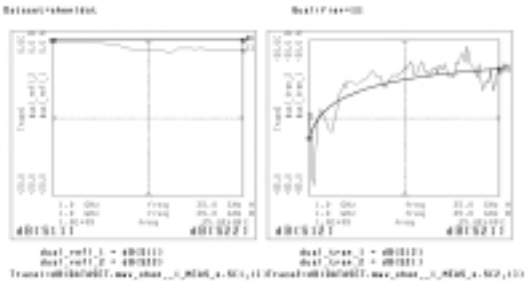

Figure 10: Comparison of S-parameter modeling with measurement data.